TRANSMISSION ELECTRON MICROSCOPE STUDY
of
WEAR IN DISK OF STANDARD C-Mn COMPOSITION

Final Report

by

E.E. Laufer and C. MacDonald

Technical University of Nova Scotia
Halifax, Nova Scotia

SSC FILE NUMBER	: 28ST.23440-6-9065
SSC CONTRACT SERIAL NUMBER	: 23440-6-9065/01-ST
PROJECT NUMBER	:
CANMET SCIENTIFIC AUTHORITY	: Dr. D.M. Fegredo

DATE : AUGUST 1987

This report should be cited as Contract Report No.:

Work on this project was conducted under the auspices of the Canada Centre for Mineral and Energy Technology, Energy, Mines and Resources, Canada

34 pp

TRANSMISSION ELECTRON MICROSCOPE STUDY
of
WEAR IN DISK OF STANDARD C-Mn COMPOSITION

FINAL REPORT

by

E.E. Laufer and C. MacDonald

Technical University of Nova Scotia
Halifax, Nova Scotia

CONTENTS

1. INTRODUCTION 1

2. PROCEDURE and NOMENCLATURE 1
   2.1. Optical Metallography 1
   2.2. TEM 2

3. OBSERVATIONS 2
   3.1. Optical Microscopy 2
   3.2. TEM 3
      3.2.1. GF Sections, 250-1000μm 3
      3.2.2. GC Sections, 250-1000μm 3
      3.2.3. HQ Sections, 250-1000μm 4
      3.2.4. GF Sections, 50-150μm 4
      3.2.5. GC Sections, 50-150μm 5
      3.2.6. HQ Sections, 50-150μm 6
      3.2.7. GF Sections, 0-25μm 6
      3.2.8. GC Sections, 0-25μm 6

4. DISCUSSION and CONCLUSIONS 7

5. REFERENCES 8

FIGURE PAGES 9

1. INTRODUCTION

In earlier work, [1,2] observations on the wear behaviour of certain experimental and standard rail steels, both from the field and from laboratory simulations were presented. Missing from the earlier work were observations of the wear behaviour of a rail steel of standard composition, tested in the laboratory rail wear simulator. It was therefore decided to examine discs of standard composition, tested under "full sequence" tests in the laboratory simulator, as described in [1] and [2]. The present observations now complete a set, including standard and premium rail, each tested in the field (FAST) and in the laboratory.

2. PROCEDURE and NOMENCLATURE

The steels examined were designated C36, L and N. Their compositions were:

C36: 0.76 C, 0.85 Mn, 0.26 Si, 0.015 S, 0.014 P, 0.01 Cr.
L: 0.73 C, 0.74 Mn, 0.35 Si, 0.006 S, 0.005 P.
N: 0.67 C, 0.88 Mn, 0.28 Si, 0.02 S, 0.012 P.

The regions examined were half way between the gauge corner and the centre of the running surface of the rail (HQ), gauge corner (GC) and gauge face (GF). While the main body of observations was confined to Transmission Electron Microscopy (TEM), some optical microscopy was also done to monitor the depth of significant deformation. Measurements of pearlite spacing made from individual micrographs are cited as apparent pearlite spacings to indicate the uncertainty arising from the limited sampling area of a single micrograph. In this work, the term "pearlite spacing" is used to indicate the repeat distance of a cementite-ferrite unit.

2.1. Optical Metallography

When pearlitic steel is etched in nital, a film covers the surface of the sample. This film appears to be epitaxial, and optically anisotropic. Thus, when such a sample is examined between crossed polars, contrast is observed which may be related to the orientations of the underlying ferrite grains or to the orientations of the cementite lamellae [3]. A very light etch gives a strong contrast, and regions where the cementite lamellae are similarly oriented are immediately recognizable as a bands or regions of a single shade. Thus, highly deformed regions are rendered in strong contrast. If a full wave plate is introduced between the polarizer and the sample, the effect is visible in a range of beautiful colours. Figures 2-5 below were taken in this way.

2.2. TEM

TEM samples were prepared as already described in [1] and [2]. As before, difficulty was experienced with surface cracks (Figure 1). These led to separation of the nickel electrodeposit from the steel surface on thinning of the TEM sample discs, making the production of surface samples very uncertain. In addition, electrochemical interference of the nickel deposit with the underlying iron led to relatively thick samples on the nickel side of the final perforation of the TEM discs, again interfering with the production of good samples near the surface. Thus, relatively few samples very near the surface were produced. Samples were examined at nominal depth ranges of 0-25μm, 50-150μm and 250-1000μm.

Almost all diffraction patterns were taken using a selected area of 3.5μm diameter. Thus, the appearance of ring diffraction patterns indicates polycrystalline material with a grain size substantially finer than 3.5μm. Texture is indicated in many of the diffraction patterns by rings whose density is unequal around their circumference.

3. OBSERVATIONS

3.1. Optical Microscopy

Figure 1 shows a portion of sample C36. The cracks seen are typical of both full size rail and rails previously examined which had been tested in the 1:10 scale facility at NRC Vancouver [1,2]. The cracks have generally been associated with MnS inclusions, and where they occur very close to the surface they are responsible for the separation of the nickel electrodeposit used for edge preservation in TEM sample preparation.

Figures 2-5 are taken between crossed polars, to emphasise effects associated with the orientations of the cementite lamellae. Thus, both grain size and the extent of the heavily deformed regions are clearly indicated. Figure 2 shows a part of the HQ section of sample C36. Note the heavily deformed region near the surface. The thickness of this region is of the order of 100μm, which corresponds well with that determined by TEM. Figures 3,4 and 5 are similar micrographs showing, respectively, region GC of sample C36 and regions HQ and GC of sample L.

3.2. TEM

3.2.1. GF Sections, 250-1000μm

All samples examined at any section appeared virtually undeformed at 1000μm although quite significant deformation was often observed as the 250μm limit of the 250-1000μm range was approached. However, the gauge face samples examined generally appeared practically undeformed at any depth. These samples were taken from samples L and N, which both showed deformation similar to that shown in Figure 5, i.e., no gauge face wear was observed, rather a build up of material due to plastic flow of metal from the running surface. Due to the difficulty in locating precise regions in the very small disc samples, the regions examined may sometimes in fact have come from lower down on the gauge face than this built up region. Micrographs from the built up region might be included among the gauge corner (GC) figures. Thus, Figures 6-8 show essentially undeformed pearlite at 1000μm. The pearlite spacing indicated in Figure 7 is approximately 440nm.

3.2.2. GC Sections, 250-1000μm

Figures 9-14 are typical of the observations made on the gauge corner sections at depths between 250 and 1000μm. Figure 9 shows the gauge corner region of sample N at 1000μm. Subgrain formation and some piling up of dislocations against the cementite lamellae are clearly seen, indicating that there has already been deformation at this depth in the gauge corner section of the disc. The apparent pearlite spacing in this micrograph is about 250nm. Figure 10 is the diffraction pattern corresponding to Figure 9 and shows a still relatively single crystal pattern, with only slight subgrain development.

Figure 11 shows sample L, GC at 550μm. Note the finer pearlite spacing here than at 1000μm, about 140nm compared to 250nm in Figure 9. The sample is also polycrystalline at this depth, which is clearly indicated by the diffraction rings seen in Figure 12, in contrast to the spots seen in Figure 10.
Continuing towards the surface, Figure 13 shows sample L, GC at 280μm. The microstructure is now broken, hardly recognizable as pearlite. A pearlite spacing is no longer a useful description of the microstructure, although regions of pearlite as fine as about 90nm are visible in the micrograph. The sample is again fine polycrystalline, with a grain size finer than that

observed at 550µm, indicated by the more complete and continuous diffraction rings. The area selected for diffraction was of 3.52µm diameter, so that the grain size is much finer than this. Figure 14 is the diffraction pattern corresponding to Figure 13.

3.2.3. HQ Sections, 250-1000µm

Figures 15-22 are typical of the observations made at the HQ section at depths between 250 and 1000µm. These sections more than any of the others examined resembled the standard rail samples from FAST reported on in [2], in particular in the observation of numerous broken cementite lamellae in an otherwise still quite recognizable pearlite.

Figure 15 shows sample N, HQ, at a depth of 1000µm. The practically undisturbed pearlite here shows that the depth of deformation was less than at the gauge corner. Pearlite spacing cannot be accurately measured in this micrograph as the cementite lamellae are tilted to the plane of the foil, but other micrographs in the series give an apparent spacing of about 400nm, similar to that shown in Figure 7. The diffraction pattern, Figure 16, is substantially single-crystalline over the selected area.

The next two figures, Figures 17 and 18, show region HQ at about 230µm. These micrographs resemble many of those seen in the full size standard rail described in [2] with their broken cementite lamellae. Some pearlite refinement has also taken place, and the micrographs indicate a variable pearlite spacing averaging about 200nm. Figure 19 is the diffraction pattern corresponding to Figure 18, and is typical of diffraction patterns from such regions, indicating a fine grained textured polycrystal.

Besides broken cementite, the HQ region at this depth also showed regions with bent pearlite as in Figure 20. Some regions were less deformed, but here also deformation led to polygonisation and there was evidence of dislocations piled up against cementite, as in Figure 21.

3.2.4. GF Sections, 50-150µm

Figures 22 and 23 are typical of the discs examined in this region. Little or no polygonisation was observed, neither was there any marked tendency to see

dislocations piled against cementite, although the dislocation density was greater than in virgin pearlite. The apparent pearlite spacing here is about 260nm in contrast to the original 440μm, i.e., there has been deformation, possibly at higher temperature than elsewhere due to flange contact. However, as stated in section 3.2.1, the gauge face samples generally showed much less signs of deformation than other samples.

3.2.5. GC Sections, 50-150μm

Figure 24 shows sample L at 155μm. It is not so different from Figures 11 or 13 at 550 and 280μm, respectively, so that while Figures 11 and 13 show a clear progression to more severe deformation as the surface is approached, Figure 24 suggests some variation in this pattern, most likely as a function of the precise location on the gauge corner from which the sample was cut. The diffraction pattern Figure 25, shows this particular region to be less polygonized than those shown in Figures 11 or 13. Thus, some variation certainly exists, but Figure 25 may be atypical in its relatively small amount of polygonization.

With Figures 26 to 32 we move closer to the surface, to the 35 to 50μm region. Figure 26, at 40μm, shows quite uneven microstructure and deformation. The diffraction patterns Figures 27 and 28 show that the polygonization is finer in the region of continuous pearlite than in the region of broken pearlite (Figure 26, lower left corner). This is consistent with, for example, the micrographs of Figures 9 and 11, where we see that the polygonization proceeds from the formation of subgrains between pearlite lamellae. The subgrains then become more misoriented with respect to each other and become finer, being ultimately limited on their sides by cementite lamellae and on the ends by grain boundaries, developed from the earlier sub-boundaries. Thus, the fine deformed pearlite is associated with fine grains.

Figure 29 is similar to Figure 26. In both cases, the pearlite spacing is about 72nm.

Figure 30 shows the gauge corner at 35μm. This depth, 35 - 40μm, seems to be about the limit for pearlite, i.e., cementite, deformation in the steels here under examination. One can no longer really speak of a pearlite "spacing", although regions of lamellae spaced about 40nm are still recognizable. The diffraction

pattern, Figure 31, shows a very fine grain size and the presence of a weak texture. Figure 32 at 50μm again shows uneven deformation and is comparable in this regard to Figure 26.

3.2.6. HQ Sections, 50-150μm

Figure 33 shows an HQ sample at 150μm. The region shown appears relatively undeformed compared to, say, Figures 17 and 18 somewhat deeper down at 230μm, which show significant amounts of broken cementite. At 100μm, Figure 34, we again see pearlite, apparently little deformed. However, the average pearlite spacing is now about 164nm, compared to the original approximately 400nm, and the diffraction pattern, Figure 35, shows a fine grained and textured ferrite matrix.

Moving closer to the surface, Figure 36 and the corresponding diffraction pattern, Figure 37, show a typical HQ section at 50μm from the surface. Here, cementite lamellae are broken into relatively short segments and the matrix is heavily dislocated. The diffraction pattern again confirms a fine grain size, but in this particular region only a relatively weak texture. The micrographs, Figures 36 and 37 are hardly distinguishable from Figures 30 and 31, GC at 35 μm.

3.2.7. GF Sections, 0-25μm

As discussed in section 3.2.1, the discs examined generally do not appear to show any significant gauge face deformation. Thus, Figures 38-40 show only slight deformation as evidenced by a certain accumulation of dislocations.

3.2.8. GC Sections, 0-25μm

No micrographs were obtained in this depth range. Samples examined in the 25-35μm range were similar to Figures 30 and 31 and there seems no reason to expect a significant change between here and the surface.

3.2.9. HQ Sections, 0-25μm

No samples were obtained in this depth range. Microstructures similar to Figures 36-37 are expected.

4. DISCUSSION and CONCLUSIONS

Perhaps the most reassuring observations of this series are those of Figures 17-20, showing broken and bent pearlite as seen in the real rail samples. Thus, the observations of the steel deformed in the 1/10 scale rail wear simulator are generally similar to those made on full size rail [2], although there are differences in detail which may derive more from the precise nature of the experiments done in the field (FAST) and on the simulator.

The rather remarkable absence of evidence of apparent deformation on the gauge face reported in the present work is also consistent with work reported earlier, especially on full size rail [2,4]. In the present work, this could be in part due to inaccurate sampling as discussed above, but the fact that the full size rail described in [2] showed the same apparent lack of deformation suggests that the observation cannot be so easily dismissed. One possibility is that flange/gauge-face contact in curves could produce rather high temperatures at the contact surfaces, and these may lead to hot deformation taking place here in contrast to the cold work taking place elsewhere. This raises the possibility that the steel which gives the best wear performance at the gauge corner and quarter sections of the running surface may not be optimum to resist gauge face wear, and vice versa.

Also, due in part to the relatively small amount of data and in part to the fact that three different steels of somewhat different compositions were examined in the present work, little can be said about the precise relationship between pearlite spacing and hardness, except that in a general way, as pearlite spacing decreases, the hardness increases. The earlier report [2] examined this question in more detail, but concluded that none of the theoretical models to be found in the literature gave a good description of the relationship between pearlite spacing and hardness. The earlier conclusions that originally fine pearlite deforms to a finer and thus harder surface layer than does originally coarser pearlite are still supported. This is consistent with the observations of Langford [5] that fine cementite is ductile while coarse cementite is brittle. It is thus of interest to produce a rail steel of a pearlitic microstructure which is sufficiently fine that the cementite is relatively ductile. Such a steel can deform at the surface to give a hard, wear resistent upper layer. Experience seems to show that this condition is reached once an initial hardness of about HRC 38 is reached [6].

The questions of texture formation did not form a part of this study, but have been addressed in a preliminary way in [7].

5. REFERENCES

1. Laufer, E.E. and C. MacDonald, Transmission Electron Microscopy Study on the Effects of Simulated Rail Loading on an Experimental Premium Rail Steel, SSC Contract Report No. OSU81-00231, December 31, 1983.

2. Laufer, E.E. and C. MacDonald, Transmission Electron Microscopy Study on the Effects of Simulated Rail Loading on an Experimental Premium Rail Steel, SSC Contract Report No. OSU81-00231, May, 1985.

3. Vander Voort, Metallography, Principles and Practice, McGraw-Hill, 1984

4. Steele, R.K., personal communication, 1987

5. Langford, G., Deformation of Pearlite, Met. Trans. A., 861-875 (1977)

6. Kalousek, J., D.M. Fegredo and E.E. Laufer, The Wear Resistance and Worn Metallography of Pearlite, Bainite and Tempered Martensite Rail Steel Microstructures, in Wear of Materials 1985, p212. K.C. Ludema, ed., ASME 1985

7. Laufer, E.E. and H. Krause, Textures in Worn Rail, Proceedings of ACOT Conference, Sarnia, May 1987; National Research Council Canada, Vancouver, May 1987

FIGURE PAGES

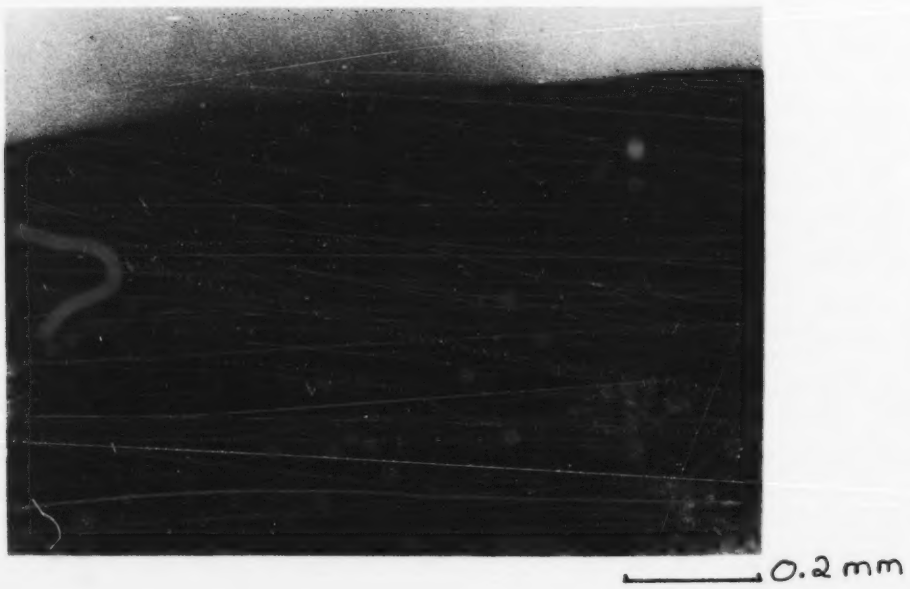

Figure 1. Sample C36. Optical micrograph, un-etched, bright field. Note cracks. (Neg. D 14)

Figure 2. Sample C36. Optical micrograph, crossed polars. Note textured region near surface. (Neg. 17.06.87-5)

Figure 3. Sample C36. Optical micrograph, crossed polars. Note heavily deformed textured region at Gauge Corner. (Neg. 17.06.87-6)

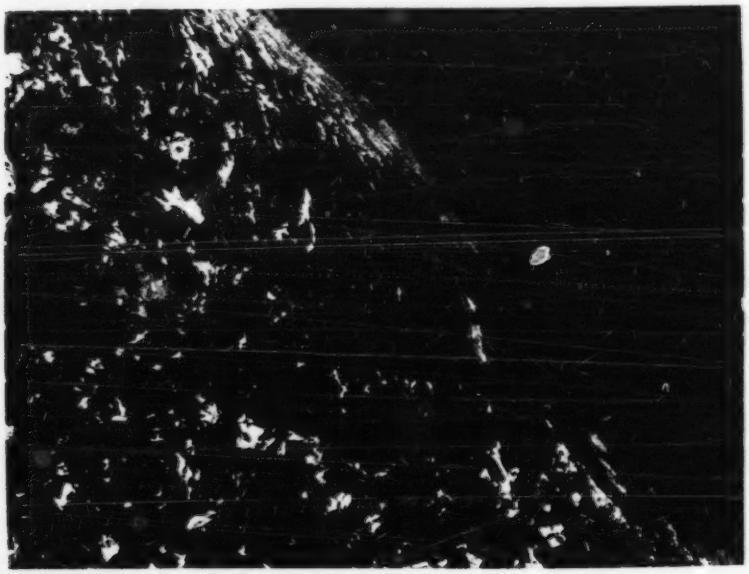

Figure 4. Sample L. Optical micrograph, crossed polars. Note textured region near surface. (Neg. 02.07.87-3)

Figure 5. Sample L. Optical micrograph, crossed polars. Note heavily deformed textured region at Gauge Corner, also limited extent of Gauge Face deformation. (Neg. 02.07.87-5)

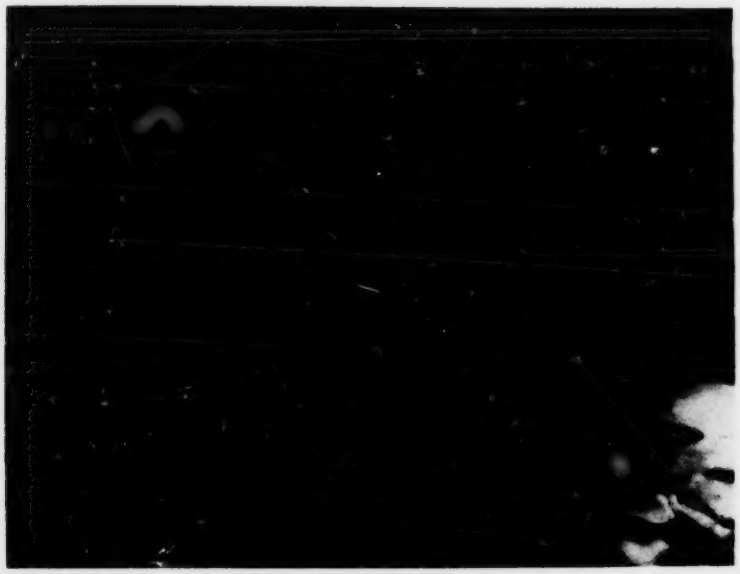

1.0 μm

Figure 6. Sample N, GF, 1000μm. Note virtually undisturbed pearlite. (Neg. 3713)

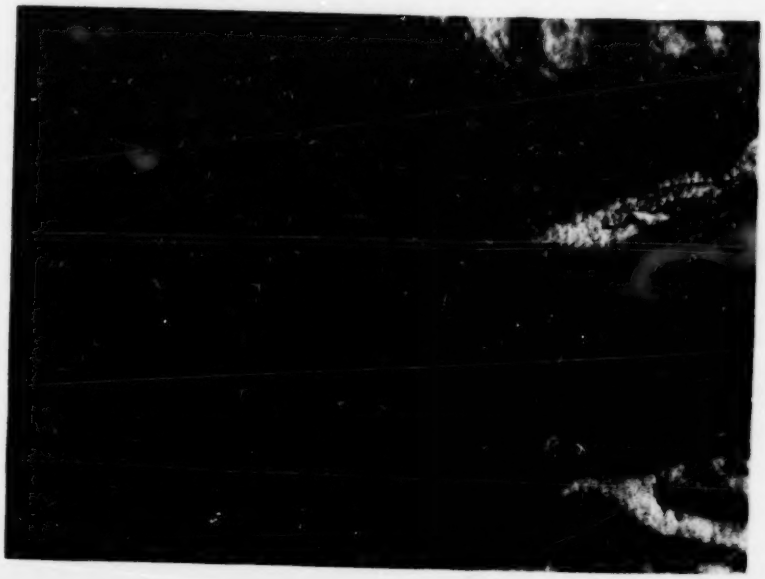

Figure 7. Sample N, GF, 1000μm. Similar to Figure 6. (Neg. 3691)

Figure 8. Diffraction pattern corresponding to Figure 7. (Neg. 3692)

1.0μm

Figure 9. Sample N, GC, 1000μm. Note subgrain formation and dislocations piled against cementite. (Neg. 3710)

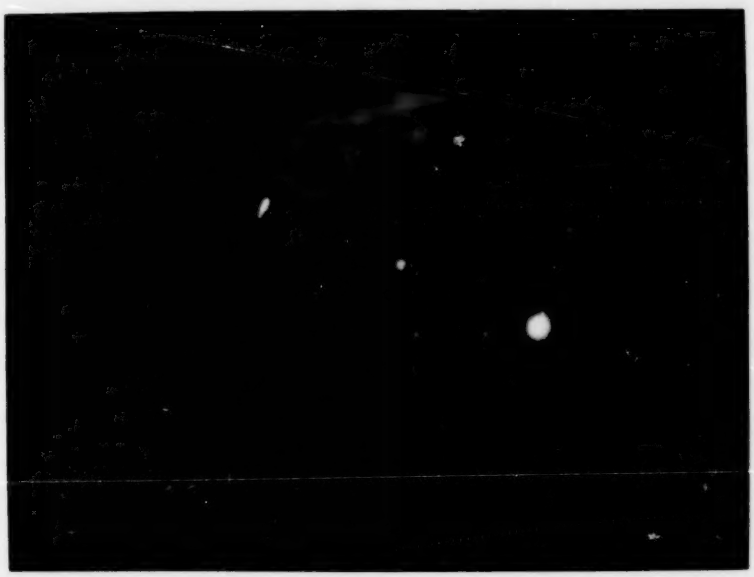

Figure 10. Diffraction pattern corresponding to Figure 9. (Neg. 3712)

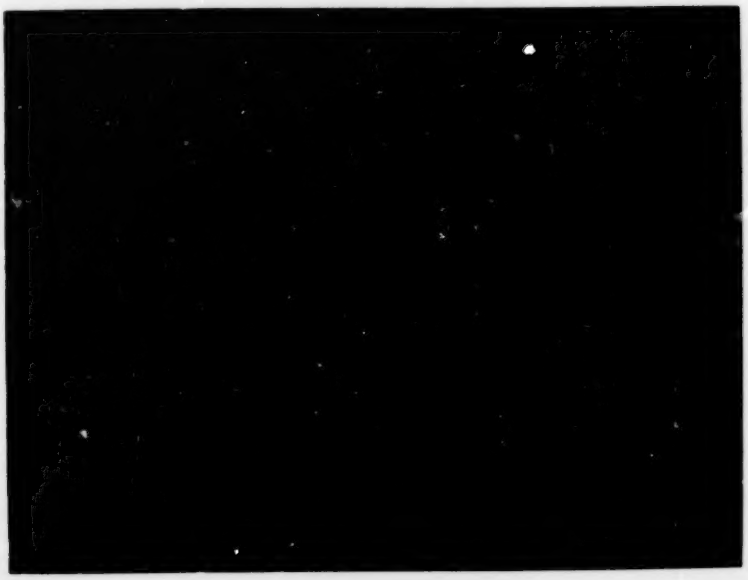

1.0μm

Figure 11. Sample L, GC, 550μm. Note finer pearlite spacing than Figure 9. Polycrystalline. (Neg. 3804)

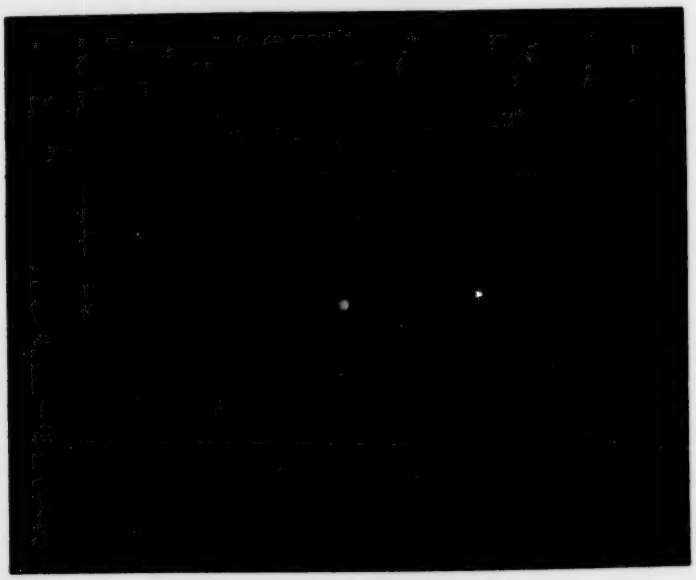

Figure 12. Diffraction pattern corresponding to Figure 11. Neg. 3805)

Figure 13. Sample L, GC, 280μm. Microstructure is broken, hardly recognizable as pearlite. (Neg. 3870)

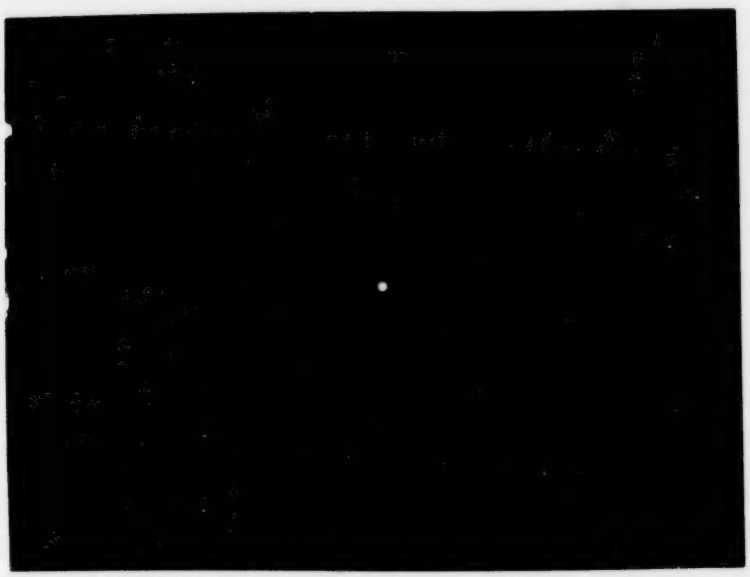

Figure 14. Diffraction pattern corresponding to Figure 13. (Neg. 3871)

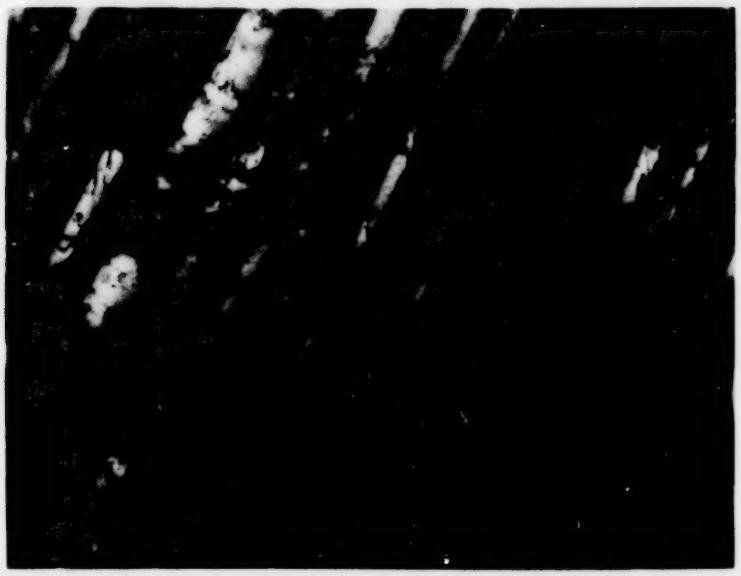

Figure 15. Sample N, HQ, 1000μm. Note practically undisturbed pearlite. (Neg. 3693)

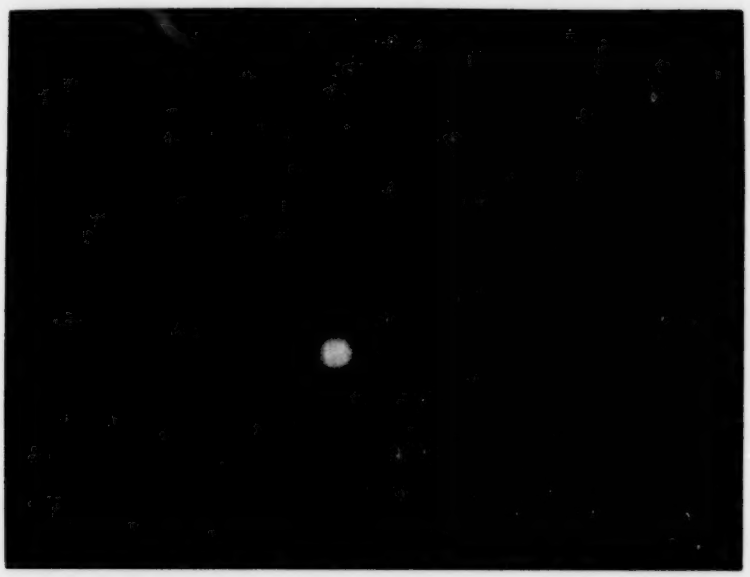

Figure 16. Diffraction pattern corresponding to Figure 15. (Neg. 3694)

1.0μm

Figure 17. Sample C36, HQ, 230μm. Note broken cementite lamellae. (Neg. 3648)

1.0μm

Figure 18. Sample C36, HQ, 230μm. Broken cementite lamellae, similar to Figure (Neg. 3642)

Figure 19. Diffraction pattern corresponding to Figure 18. (Neg. 3643)

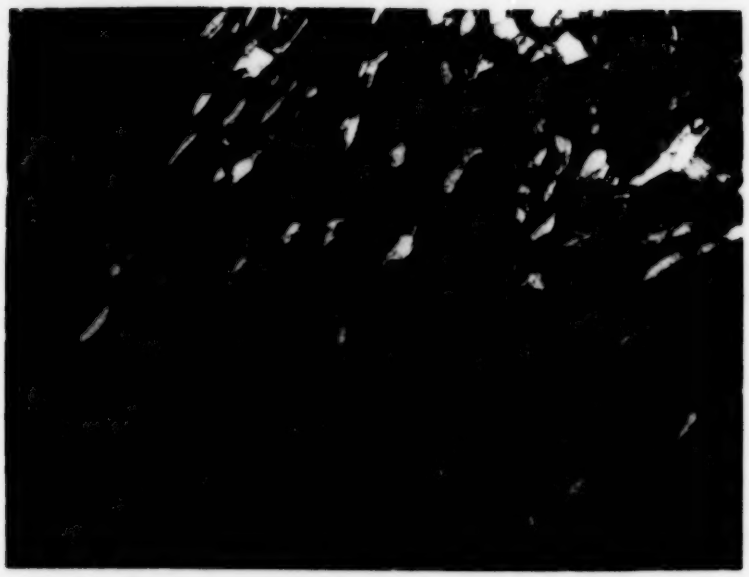

Figure 20. Sample C36, HQ, 230μm. Note bent cementite lamellae. (Neg. 3651)

0.5 μm

Figure 21. Sample C36, HQ, 230μm. Typical polygonisation pattern, perpendicular to cementite, with dislocations piled against cementite lamellae. (Neg. 3836)

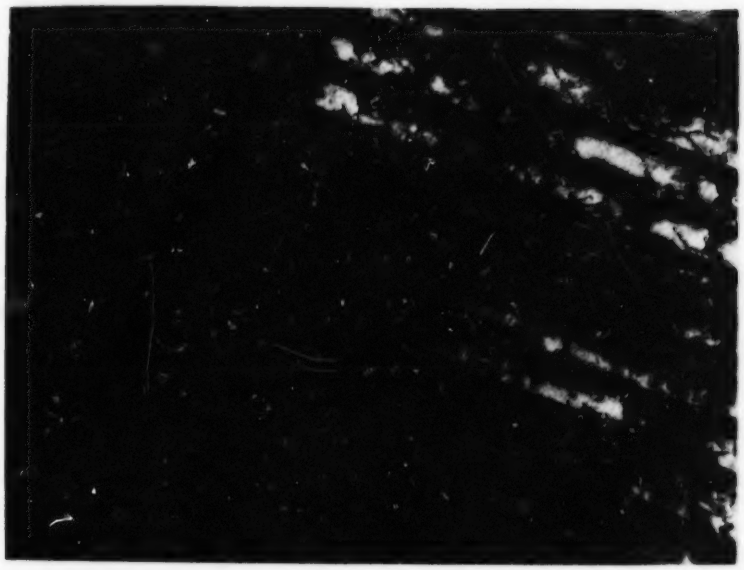

Figure 22. Sample L, GF, 100μm. Dislocation buildup, no polygonisation or pile ups. (Neg. 3770)

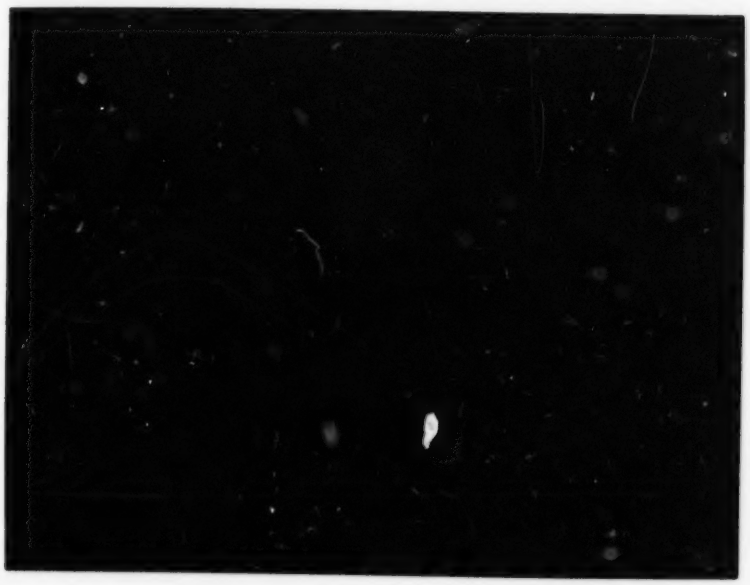

Figure 23. Diffraction pattern corresponding to Figure 22. (Neg. 3771)

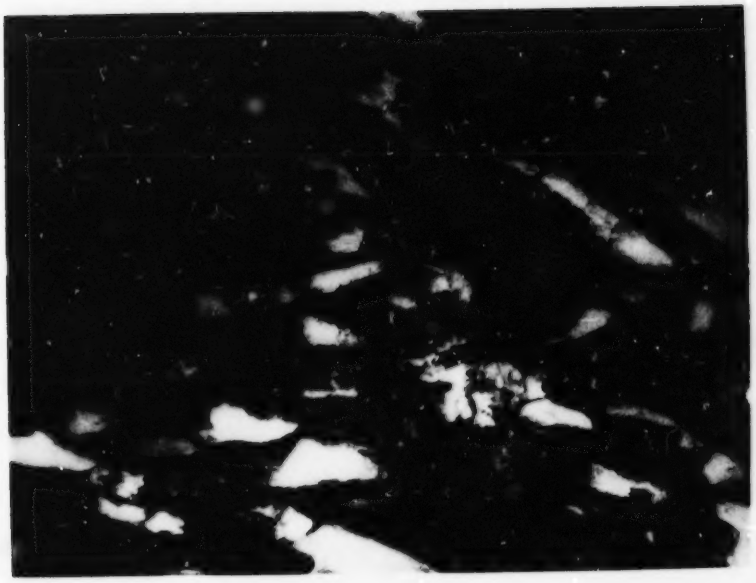

1.0μm

Figure 24. Sample L, GC, 155μm. Polygonisation into subgrains apparent. (Neg. 3802)

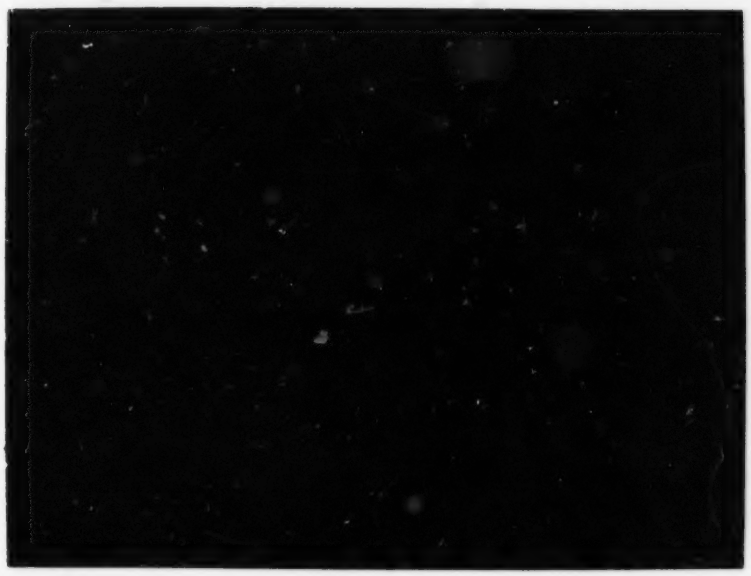

Figure 25. Diffraction pattern corresponding to Figure 24. (Neg. 3803)

1.0μm

Figure 26. Sample L, GC, 40μm. Note uneven deformation. (Neg. 3781)

Figure 27. Diffraction pattern corresponding to continuous pearlite region of Figure 26. (Neg. 3782)

Figure 28. Diffraction pattern corresponding to broken pearlite region of Figure 26. (Neg. 3783)

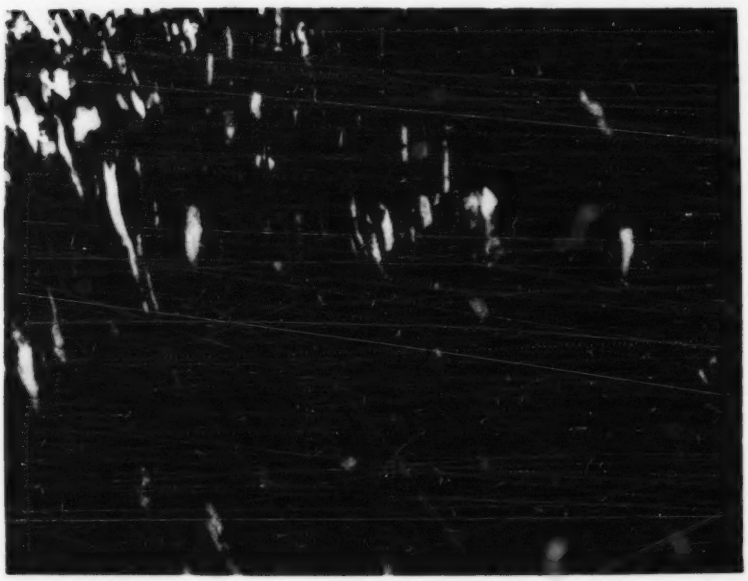

Figure 29. Sample L, GC, 40μm. Compare Figure 26. (Neg. 3784)

Figure 30. Sample C36, GC, 35μm. Pearlite fractured almost beyond recognition, heavily dislocated. (Neg. 3671)

Figure 31. Diffraction pattern corresponding to Figure 30. (Neg. 3669)

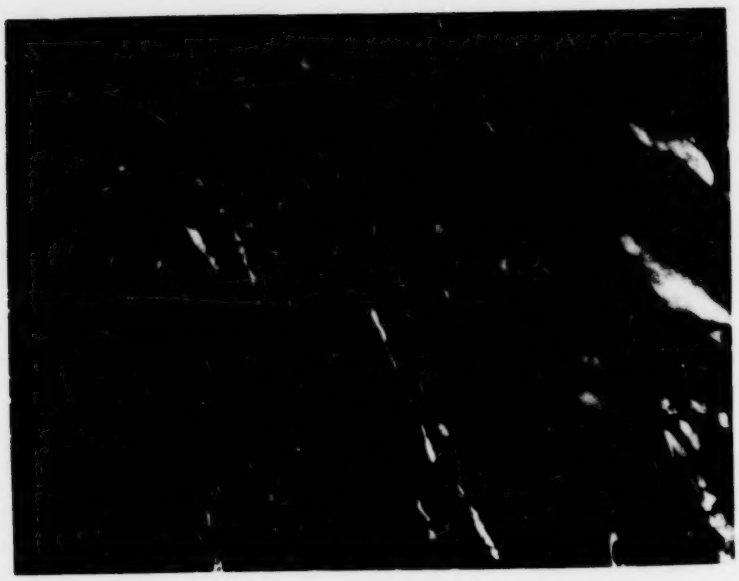

0.5μm

Figure 32. Sample C36, GC, 50μm. Uneven deformation. Compare Figure 26. (Neg. 3675)

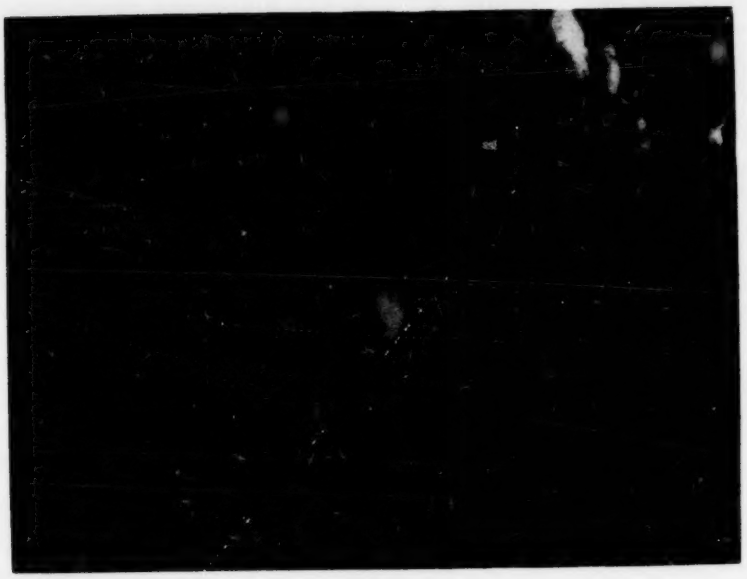

1.0μm

Figure 33. Sample L, HQ, 150μm. Relatively undeformed pearlite. Polygonisation beginning. (Neg. 3826)

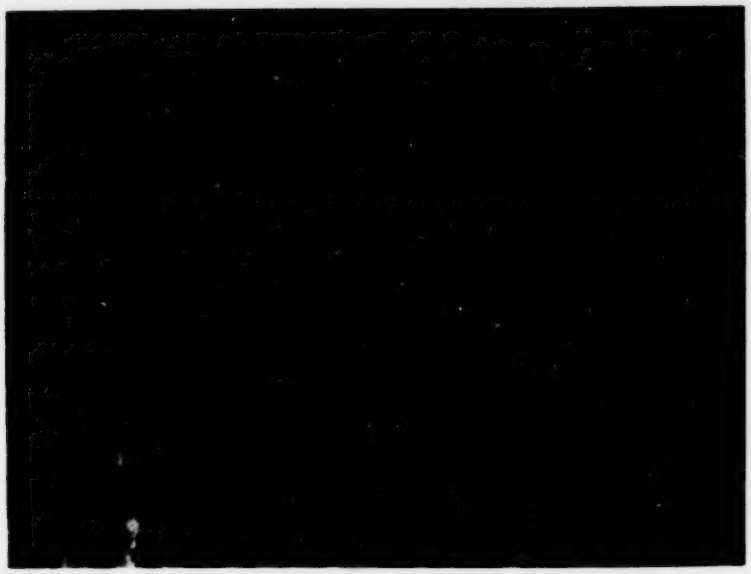

Figure 34. Sample C36, HQ, 100μm. Sample shows significant polygonisation. (Neg. 3654)

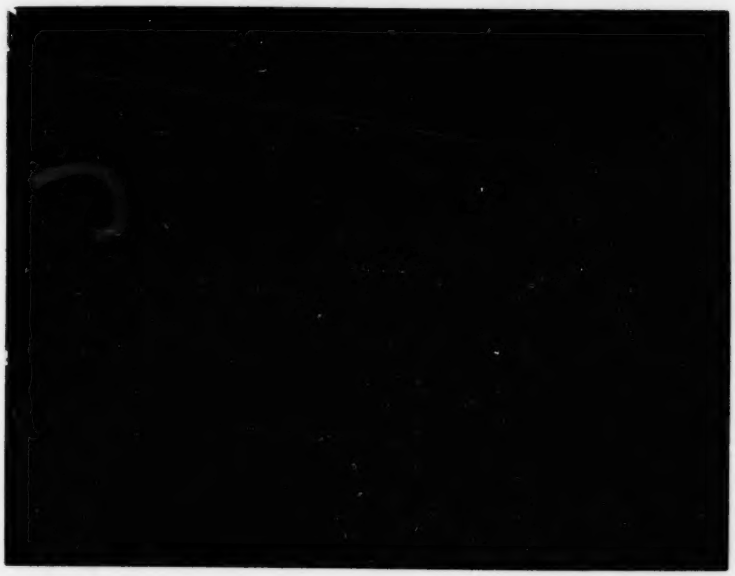

Figure 35. Diffraction pattern corresponding to Figure 34. (Neg. 3655)

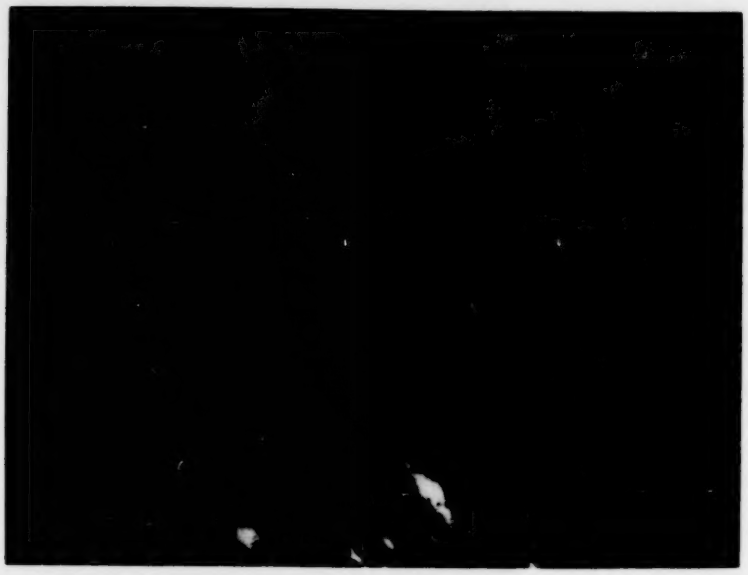

Figure 36. Sample L, HQ, 50μm. Pearlite broken, almost unrecognizable. (Neg. 3860)

Figure 37. Diffraction pattern corresponding to Figure 36. (Neg. 3861)

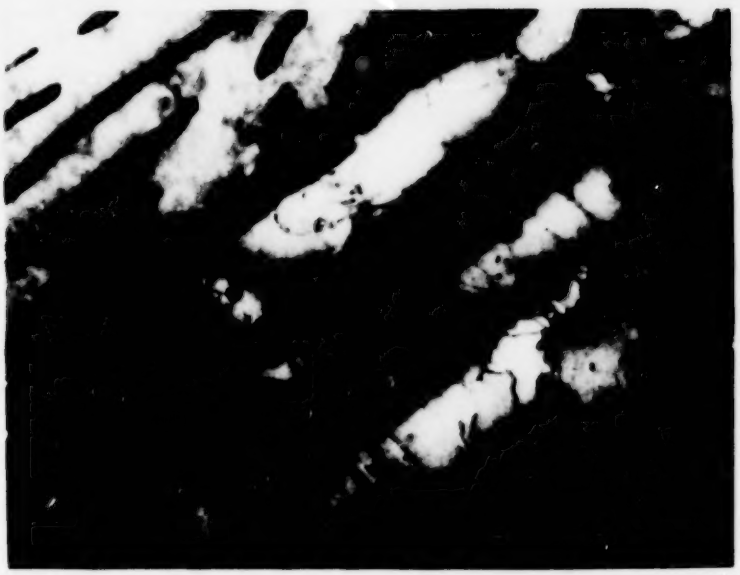

0.5μm

Figure 38. Sample L, GF, 20μm. Minimal deformation apparent, dislocations piled against cementite. (Neg. 3745)

0.5μm

Figure 39. Sample L, GF, 20μm. Detail, showing piling up of dislocations against cementite and beginning subgrain formation. (Neg. 3748)

Figure 40. Diffraction pattern corresponding to Figure 38. (Neg. 3747)